Journal of Magnetism and Magnetic Materials 541 (2022) 168552

Contents lists available at ScienceDirect

Journal of Magnetism and Magnetic Materials

journal homepage: www.elsevier.com/locate/jmmm

Research articles

Tunnel magnetoresistance detection of skyrmions

Hao Chen, William Bouckaert, Sara A. Majetich *

Physics Department, Carnegie Mellon University, Pittsburgh, PA 15213, USA

ARTICLE INFO

Keywords:
Skyrmion
Magnetoresistance
Racetrack memory
Magnetic tunnel junction

ABSTRACT

Micromagnetic simulations are used to investigate different strategies for tunnel magnetoresistance detection of the Néel skyrmion core direction and Bloch skyrmion chirality. When a Néel skyrmion passes beneath a perpendicularly magnetized dot separated by a tunnel barrier, a peak or dip in the tunnel magnetoresistance as a function of time reveals the core direction. When a Bloch skyrmion travels below a synthetic antiferromagnet, magnetized in-plane with an axis perpendicular to that of the track, the tunnel magnetoresistance as a function of time shows a peak followed by a dip, or vice versa, depending on the chirality. The results are compared with existing detection methods based on the Hall resistance.

1. Introduction

Skyrmions are stable non-collinear spin patterns [1,2] that were later proposed for use as 1's and 0's in racetrack memory [3–5]. They have also been investigated for use as synapses for neuromorphic computing [6–8], for reservoir computing [9], and for dynamic magnonic crystals [10]. For this to work, it must be possible to uniquely detect the passage of a skyrmion as well as features that could be used to represent 1's and 0's, such as the magnetization direction of the core or the chirality for a Bloch skyrmion. Bloch skyrmions are particularly interesting due to their topological protection. The prior micromagnetic simulations have focused on the dynamics within the skyrmionic layer rather than the details of detection. Experimentally, detection has proved to be quite challenging. While skyrmions have been imaged by scanning transmission x-ray microscopy [11–13], spin polarized scanning tunneling microscopy [14], and Lorentz transmission electron microscopy [2,15], there are still many questions about the best way to detect them electronically – a requirement for practical racetrack memory. The most promising approaches so far have used the transverse voltage due to the Hall effect, but the signal is still very weak [16–18]. Here we use simulations to examine alternative vertical detection methods using magnetoresistance between the skyrmion racetrack and a uniformly magnetized detector dot above it. With a tunnel barrier between the dot and skyrmion stack, the interactions are magnetostatic and there is less distortion of the skyrmion due to the detector dot than with an all-metallic configuration and giant magnetoresistance (GMR). Tunnel magnetoresistance (TMR) also promises a larger signal-to-noise ratio than GMR, and so we focus on this approach. If the vertical tunnel current through a magnetic detector dot is dominated by the magnetization pattern directly below the tunnel barrier (i.e., in the skyrmion racetrack), then the dynamics of the TMR signal can reveal whether a skyrmion is present or not, the direction of its core, and in the case of a Bloch skyrmion, its chirality. We examined two different types of skyrmion racetrack/detector dot systems: 1) a circular dot with perpendicular (vertical) magnetization to determine the core direction for a Néel skyrmion, and 2) a rectangular dot made of a synthetic antiferromagnet (SAF) with in-plane magnetization perpendicular to the racetrack axis to determine the chirality of a Bloch skyrmion.

The TMR skyrmion detector involves a ferromagnetic electrode (the dot detector) separated from a multilayer skyrmionic racetrack by a thin tunnel barrier. A current is applied longitudinally to drive the skyrmion along the racetrack. A small amount of current is picked off to pass vertically across the insulating barrier, leading to TMR between the racetrack and the detector. A schematic of the circuit is shown in Fig. 1.

2. Materials and methods

COMSOL Multiphysics software was used to simulate the current density profile in the skyrmion racetrack, to verify that the vast majority of the current passing upward across the tunnel barrier comes from the racetrack volume located directly below the contact. A voltage difference of 660 mV was applied along the racetrack (x-axis) to generate a current density $J_x = 10^{12}$ A/m^2. Next Mumax^3 software [19] was used to simulate the spin configurations, including the mutually interacting stray fields of the skyrmion and dot detector, as well as the trajectories of the skyrmions driven by spin polarized current along the racetrack. The

* Corresponding author.
E-mail addresses: haochen2@andrew.cmu.edu (H. Chen), wbouckae@andrew.cmu.edu (W. Bouckaert), sara@cmu.edu (S.A. Majetich).

https://doi.org/10.1016/j.jmmm.2021.168552
Received 7 July 2021; Received in revised form 23 August 2021; Accepted 11 September 2021
Available online 16 September 2021

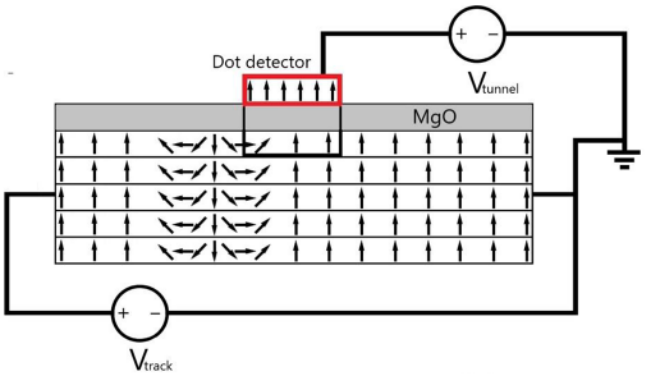

Fig. 1. Schematic side view of the skyrmion racetrack coated with a thin tunnel barrier with a ferromagnetic dot detector on top. A voltage is applied along the racetrack to create a large current density and drive the skyrmions through spin transfer torque. A separate potential difference is applied to the dot detector so that a small amount of tunnel current passes vertically from the racetrack through the dot, leading to a TMR signal that varies in time as the skyrmion passes beneath the detector (here with perpendicular magnetization). In the simulations, $V_{track} = 660$ mV and $V_{tunnel} = 330$ mV.

model Néel skyrmion was 35 nm in diameter, and passed beneath a 50 nm diameter 1 nm thick circular CoFeB detector dot with perpendicular magnetization (z), separated from the racetrack by a 1 nm thick MgO tunnel barrier. The model Bloch skyrmion was generated in the B20 material FeGe (10 nm thickness), with a 1 nm MgO tunnel barrier and a 20 nm × 50 nm synthetic antiferromagnet (SAF) detector made of two 1 nm CoFeB layers separated by a 1 nm Ru spacer. The axis of the SAF magnetization (y) was in the plane of the substrate but perpendicular to the racetrack axis (x). Further details about the simulations and materials parameters used are given in the Supplemental Material Section S1.

Using a tunnel barrier on the top of the skyrmion racetrack enables a detection of a small current but high resistance readout signal while driving skyrmions along the racetrack. A positive voltage drives electrons from the racetrack towards the detector dot. For the results shown here, the electrons were assumed to be fully polarized by the top layer of the skyrmion racetrack just beneath the detector. MATLAB software was used to calculate the local TMR for a (1 nm)^2 mesh. The TMR was assumed to follow an empirical $cos(\theta)$law [20], where theta is the angle between the magnetization in the detector dot and that in the mesh cell below it in the skyrmionic stack. A parallel resistor model was used to sum the contributions from all the cells of the detector dot and work out the device TMR. Further details are given in the Supplemental Material Figure S2.

3. Results and discussion

Fig. 2 (a) shows the geometry used to calculate the Bloch skyrmion current density profile. Fig. 2 (b-d) show the cross sections of the current density for three different cut planes within the skyrmion racetrack; $z - 9$ nm is directly below the MgO tunnel barrier. While the color scale is chosen to accentuate the degree of spatial variation, the absolute amount can be controlled by the tunnel barrier thickness. A 1 nm thick tunnel barrier this leads to spatial variations of ~ 6% in J_x in the vicinity of the detector, as shown in Figure S3 of the Supplemental Material. MgO has a resistance that could increase orders of magnitude by adding only a few angstroms of thickness. With a 100 times more resistive ($\sigma_{MgO} = 1.852$S/m) tunnel barrier, the current fluctuation are reduced to 0.06%, which is exactly 1/100 of its original value, as shown in Fig. S4 of the Supplemental Material. Similar details for the Néel skyrmion with a circular dot detector are shown in Figure S5 of the Supplemental Material.

While the presence of the TMR detector has only a small effect on current flow in the x-direction, the vertical current density is highly localized in the region directly below the contact. Fig. 2 b-d show J_z in the different cut-planes inside the racetrack and strong localization behavior was observed. For comparison, Figure S3 of the Supplemental Material shows the current inhomogeneity in J_x, and Figure S4 shows the effect of a thicker barrier. Most of the current flows in the $+x$ direction, driven by the 660 mV voltage difference, but a fraction near or under the detector will tilt towards the z direction because of the grounded detector. The electrons carried by the z component of these vectors are assumed to be polarized by the very top magnetic layer and collected by the detector, giving a current signal to detect skyrmions.

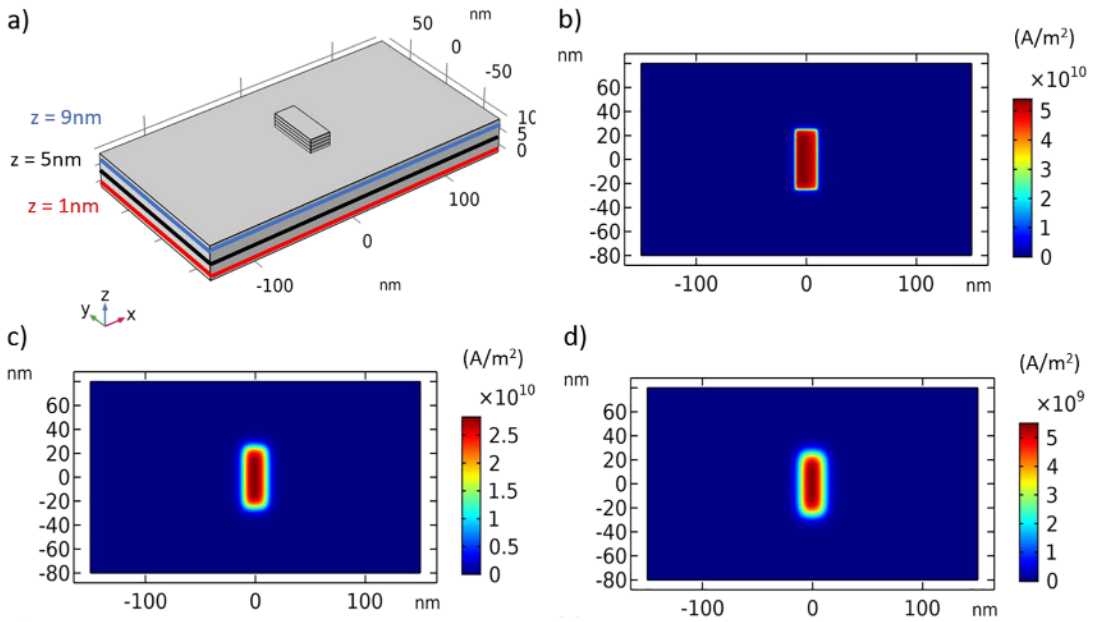

Fig. 2. (a) Geometry used in Bloch skyrmion current density simulation. Three cut planes are labeled to indicate the surface where the current density profiles are plotted. (b) – (d) show the z component of the current density at three cut planes in the skyrmion stack: (b) $z = 9$ nm, which is immediately below the MgO layer, (c) $z = 5$ nm, and (d) $z = 1$ nm near the bottom of the stack. The uniformity of the current distribution in (b) suggests that the simple parallel resistor model is a good approximation.

The uniformity of the z component of the current density also suggests that the parallel resistance model is a good approximation for this system. For the parameters given, and a 6% current fluctuation in J_x, the device resistance would be $5.4k\Omega$, but there are other considerations for actual experiments. The detector was placed at the center of the racetrack in all simulations. Acting as a voltage divider, the detector would effectively share a half of the voltage applied across the racetrack ($330mV$). This is a reasonable working voltage for an MTJ device, but the required voltage across the racetrack could go higher. At that time, the placement of the detector and the voltage applied at the top of the detector (grounded in our case) should be chosen carefully. After ensuring a reasonable working voltage for the detector, the current fluctuation induced in the racetrack should be minimized. If the tunnel barrier resistance is increased by a factor of 100, the magnitude of the current fluctuation in the x-direction would be decreased by a factor of one hundred.

Fig. 3 (a) shows the trajectory of a 35 nm diameter Néel skyrmion moving along a 400 nm × 200 nm × 1 nm racetrack passing below a 50 nm diameter perpendicularly magnetized detector dot that is separated from the skyrmionic stack by a 1 nm tunnel barrier. Here the skyrmion core is in the $+z$ direction, perpendicular to the racetrack plane. The skyrmion Hall effect causes a systematic downward tilt to the trajectory. The skyrmion Hall angle is found from the arctangent of the ratio of the velocities along and perpendicular to the driving current, which is equal to $\frac{Q}{\alpha D}$, where $Q = \pm 1$ is the topological charge of the skyrmion, $\alpha \approx 0.1$ is the Gilbert damping parameter, and D is the dissipation force [11–13]. The dissipation force $D = \frac{\pi^2 d}{8\gamma_{dw}}$ is related to the skyrmion diameter d and the energy of a domain wall $\gamma_{dw} = \sqrt{A/K}$. For exchange stiffness $A = 1.5 \times 10^{-11}$ J/m and $K - 8 \times 10^7$ J/m^3, the calculated skyrmion Hall angle is 49.2°, assuming a nonadiabaticity parameter $x_i = 1$. These simulations used a more realistic nonadiabaticity parameter and nonadiabaticity parameter of 0.2, but if x_i were one, the skyrmion Hall angle would be 46.7°, in reasonable agreement with the theoretical prediction. Previous experimental work has shown little correlation between the skyrmion size and the skyrmion Hall angle [21], which is believed to be due to small inhomogeneities that would not be present in the simulations.

When the skyrmion is far from the detector dot, the TMR approaches that for parallel or antiparallel states of a tunnel junction with uniformly magnetized layers, as shown in Fig. 4. However, there are significant deviations when the skyrmion passes near the detector dot where the local magnetization is non-uniform. The attraction or repulsion is consistent with expectations based on the force on a magnetic moment of the skyrmion core due to the spatial field gradient of the detector dot. The vertical (z) and horizontal (x) fringe fields from the detector dot are shown in the Supplemental Material Figures S6 and S7, respectively, and an explanation of how the deflection force is calculated from the field gradients is discussed and shown in Figure S8. The net field gradients, and therefore the magnetic forces, are largest near the edges of the dot, and are dominated by the spins in the core. As the stray field from the dot detector is modifying the trajectory of the skyrmion, the repulsive and attractive forces change the speed of the skyrmion when it is passing near the dot detector. There are different peak and dip times in Fig. 4 because of the difference in the background field of the racetrack where no skyrmions are present. In either case the skyrmion follows a trajectory where it has the lowest energy. While the skyrmion diameter has previously been shown to shrink as the saturation field is approached [17], we note that the core diameter increases when it passes beneath a detector dot with parallel magnetization. For our detector dot thickness, the field it generates is well below the saturation field of the skyrmionic racetrack.

To detect in-plane magnetization, and in particular the chirality of a 50 nm diameter Bloch skyrmion, a rectangular 20 nm × 50 nm synthetic antiferromagnet (SAF) structure was used. Fig. 2 (a) shows a schematic for the simulation setup. The SAF detector has a 1 nm thick bottom layer magnetized in $+y$ direction. The $-y$ magnetized top layer is separated 1 nm away from the bottom layer, representing the Ru spacer. The detected TMR was assumed to be sensitive to the racetrack area under the SAF detector only. Fig. 5 (a) shows the simulated device TMR when a Bloch skyrmion with chirality -1 is placed on the racetrack and moving across the SAF detector. The spatially resolved local TMR in the detector area is shown in Fig. 5 (b, c). Skyrmions with different chirality show different y component magnetization patterns, consistent with the overall time-dependence shown in Fig. 5 (a).

The simulations described here are case studies of model systems, and it is worth discussing both how the results could differ under less ideal conditions, how they could vary depending on the dimensions of

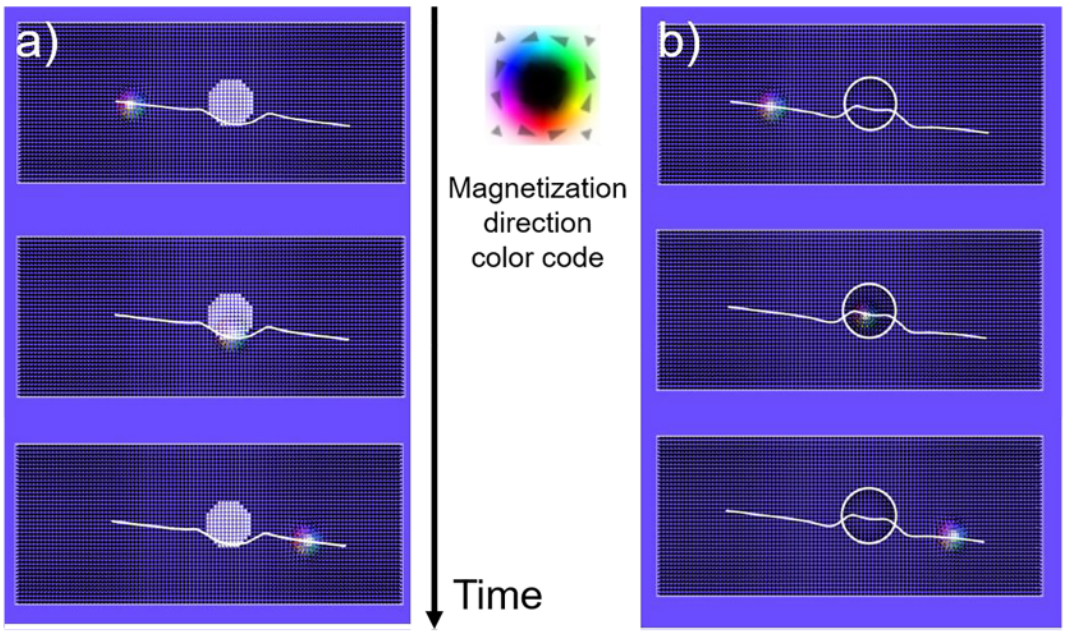

Fig. 3. (a) When the detector dot magnetization is parallel to that of the skyrmion core (both $+z$), the skyrmion has a repulsive deflection when it passes in the vicinity of the dot. (b) When the detector dot magnetization is antiparallel to that of the skyrmion core, the skyrmion has an attractive deflection when it goes by the dot.

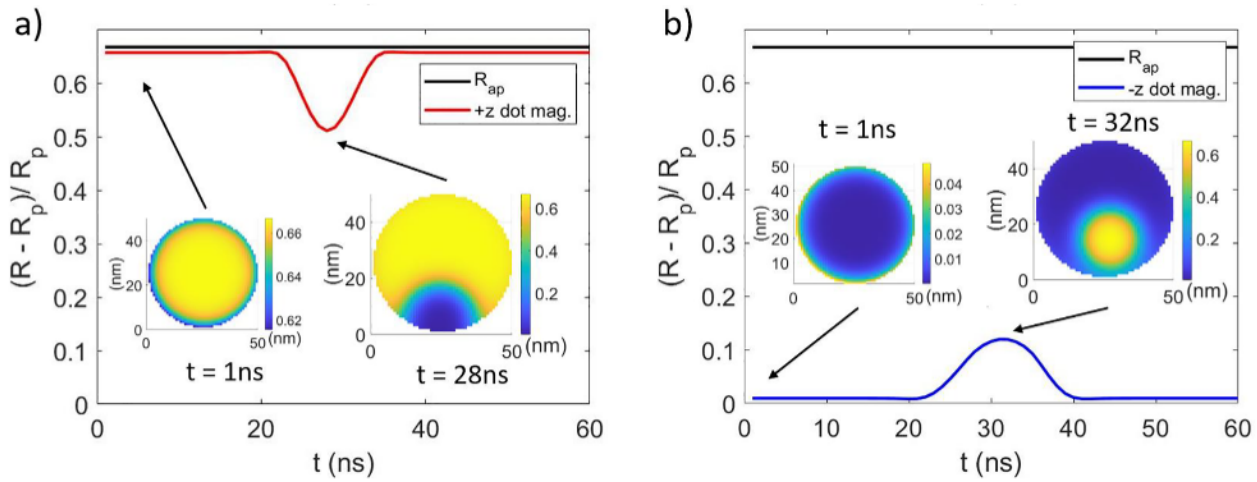

Fig. 4. TMR as a function of time for the trajectories shown in Fig. 3 for the case where the core is magnetized in the $+z$ (a) and $-z$ (b) directions. The insets show the spatial distribution of the TMR through the detector dot at different instants in time. Here the TMR was assumed to be 0.67 for a uniformly magnetized tunnel junction.

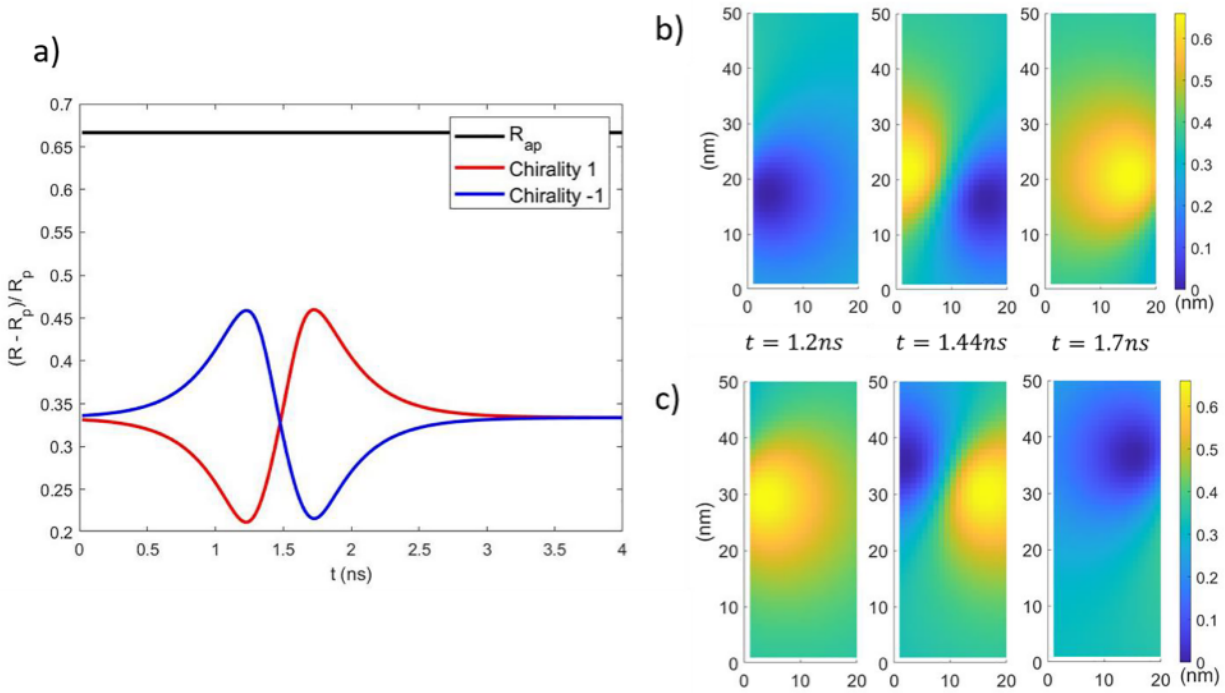

Fig. 5. (a) Simulated device TMR for Bloch skyrmions with chirality 1 and -1. In the chirality -1 condition shown in Fig. 2 (a), we first see a peak in the device TMR (blue curve), due to the antiparallel magnetization configuration between the SAF bottom layer and the skyrmion racetrack beneath as the skyrmion enters the SAF detection area. A dip is then observed due to the antiparallel magnetization as the skyrmion exits. Color maps of the pixel-by-pixel local TMR for chirality (b) 1 and (c) -1 recorded when the skyrmion is entering (1.2*ns*), at the center of (1.44*ns*) and exiting (1.7*ns*) the detected area.

the racetrack and detector dot. The size of a skyrmion can be tuned by the choice of materials parameters [22]. Efforts are underway to reduce the skyrmion diameter, but in any case, the detector dot and skyrmion dimensions would have to be comparable. We considered a Néel skyrmion with an ultrathin (1 nm) racetrack and a Bloch skyrmion with a more typical thickness (10 nm) racetrack. Experimentally, thicker multilayer skyrmion stacks have received the most attention, but thin stacks are being investigated as well [14,23]. The thickness of the perpendicularly magnetized detector dot will impact the magnitude of the skyrmion deflection, as shown in Figure S9 of the Supplemental Material. The thickness of the in-plane magnetized SAF detector is less likely to affect the detection of Bloch skyrmion chirality. The effect of differing degrees of spin polarization on the Hall angle is shown in Figure S10. The trajectories for T = 0 K are very smooth, but at room temperature (294 K) thermal fluctuations introduce a small random component, as shown in Figure S11. The jumps are small relative to the skyrmion size and fortunately do not affect the overall trajectory or ability to detect the skyrmion. A video showing the motion, size, and shape fluctuations of the skyrmion at 294 K in its trajectory over 6 ns is included in the Supplemental Material.

Finally we discuss how the results for TMR detection could compare with those for Hall magnetoresistance. Zeissler, et al. [17], who used a combination of scanning transmission x-ray microscopy and Hall resistance measurements on Pt/Co/Ir nanodiscs, and extrapolated a Hall

resistivity of 22 ± 2 nΩ – cm for single 150 ± 30 nm skyrmions. Macciarello, et al. [18] used a combination of magnetic force microscopy and Hall resistance to detect sub-100 nm skyrmions in a B20 material racetrack, measuring Hall resistivity differences of ~ 50 nΩ cm, corresponding to differences in R_{xy} of 5 mΩ. In both cases the contributions from the ordinary and anomalous Hall effects had to be taken into account. In contrast, uniformly magnetized tunnel junctions show differences of kΩ – MΩ between the fully parallel and antiparallel states [24]. This value is considerably reduced when the free layer has a non-collinear configuration such as a skyrmion, or if the spin polarization of electrons coming from the skyrmion racetrack was incomplete, but the TMR is still likely to be orders of magnitude larger than the Hall resistance.

4. Conclusions

In summary, we have used COMSOL, Mumax[3] and MATLAB software to demonstrate methods for uniquely detecting the core magnetization direction of Néel or Bloch skyrmions, and the chirality of Bloch skyrmions. The core direction of Néel and Bloch skyrmions could be detected using a dot detector magnetized in the z-direction and measuring the time dependence of the TMR as the skyrmion passes beneath. The chirality of a Bloch skyrmion can be determined by using a *y*-direction magnetized SAF detector and measuring the time dependence of the TMR. Simulations suggest that the magnitude of time-dependent changes in the TMR signal is likely to be orders of magnitude larger than the Hall effect signal, and experiments are underway to test these predictions.

Declaration of Competing Interest

The authors declare that they have no known competing financial interests or personal relationships that could have appeared to influence the work reported in this paper.

Acknowledgments

This work was supported by the US Department of Energy grant DE-SC0019237.

Appendix A. Supplementary data

Supplementary data to this article can be found online at https://doi.org/10.1016/j.jmmm.2021.168552.

References

[1] S. Muhlbauer, B. Binz, F. Jonietz, C. Pfleiderer, A. Rosch, A. Neubauer, R. Georgii, P. Boni, Skyrmion lattice in a chiral magnet, Science 323 (5916) (2009) 915–919.
[2] X.Z. Yu, Y. Onose, N. Kanazawa, J.H. Park, J.H. Han, Y. Matsui, N. Nagaosa, Y. Tokura, Real-space observation of a two-dimensional skyrmion crystal, Nature 465 (7300) (2010) 901–904.
[3] J. Sampaio, A. Fert, V. Cros, Skyrmions on the track, Nat. Nanotech. 8 (2013) 152.
[4] W. Jiang, P. Upadhyaya, W. Zhang, G. Yu, M.B. Jungfleisch, F.Y. Fradin, J. E. Pearson, Y. Tserkovnyak, K.L. Wang, O. Heinonen, S.G.E. te Velthuis, A. Hoffmann, Blowing magnetic skyrmion bubbles, Science 349 (6245) (2015) 283–286.
[5] R. Tomasello, E. Martinez, R. Zivieri, L. Torres, M. Carpentieri, G. Finocchio, A strategy for the design of skyrmion racetrack memories, Sci. Rep. 4 (2014) 6784.
[6] D. Pinna, F. Abreu Araujo, J.-V. Kim, V. Cros, D. Querlioz, P. Bessiere, J. Droulez, J. Grollier, Skyrmion Gas Manipulation for Probabilistic Computing, Phys. Rev. Appl. 9 (2018), 064018.
[7] Y. Huang, W. Kang, X. Zhang, Y. Zhou, W. Zhao, Magnetic skyrmion-based synaptic devices, Nanotechnol. 28 (2017) 1.
[8] R. Chen, C. Li, Y.u. Li, J.J. Miles, G. Indiveri, S. Furber, V.F. Pavlidis, C. Moutafis, Nanoscale room-temperature multilayer skyrmionic synapse for deep spiking neural networks, Phys. Rev. Applied 14 (1) (2020), https://doi.org/10.1103/PhysRevApplied.14.014096.
[9] G. Bourianoff, D. Pinna, M. Sitte, K. Everschor-Sitte, Potential implementation of reservoir computing models based on magnetic skyrmions, AIP Adv. 8 (5) (2018) 055602, https://doi.org/10.1063/1.5006918.
[10] F. Ma, Y. Zhou, H.B. Braun, W.S. Lew, Skyrmion-based dynamic magnonic crystal, Nano Lett. 15 (2015) 4029.
[11] S. Woo, K. Litzius, B. Kruger, M.-Y. Im, L. Caretta, K. Richter, M. Mann, A. Krone, R. M. Reeve, M. Wiegand, P. Agrawal, I. Lemesch, M.-A. Mawass, P. Fischer, M. Klaui, G.S.D. Beach, Observation of room—temperature magnetic skyrmions and their current-driven dynamics in ultrathin metallic ferromagnets, Nat. Mater. 15 (2016) 501.
[12] W. Jiang, X. Zhang, G. Yu, W. Zhang, Z. Wang, M.B. Jungfleisch, J.E. Pearson, X. Cheng, O. Heinnonen, K.L. Wang, Y. Zhou, A. Hoffmann, S.G.E. te Velthuis, Direct observation of the skyrmion Hall effect, Nat. Phys. 13 (2017) 162.
[13] K. Litzius, I. Lemesh, B. Krüger, P. Bassirian, L. Caretta, K. Richter, K. Büttner, O. A. Sato, J. Tretiakov, R.M. Förster, M. Reeve, I. Wiegand, H.S. Bykova, G. Schütz, G.S.D. Beach, M. Kläui, Skyrmion Hall effect revealed by direct time-resolved X-ray microscopy, Nat. Phys. 13 (2017) 170.
[14] N. Romming, C. Hanneken, M. Menzel, J.E. Bickel, B. Wolter, K. von Bergmann, A. Kubetzka, R. Wiesendanger, Writing and deleting single magnetic skyrmions, Science 341 (6146) (2013) 636–639.
[15] M. Li, D. Lau, M. De Graef, V. Sokalski, Lorentz TEM investigation of chiral spin textures and Néel skyrmions in asymmetric $[Pt/(Co/Ni)_m/Ir]_n$ multi-layer thin films, Phys. Rev. Mater. 3 (2019), 064409.
[16] X. Zhang, G.P. Zhao, H. Fangohr, J.P. Liu, W.X. Xia, J. Xia, F.J. Morvan, Skyrmion-skyrmion and skyrmion-edge repulsions in skyrmion-based racetrack memory, Sci. Rep. 5 (2015) 7643.
[17] K. Zeissler, S. Finizio, K. Shahbazi, J. Massey, F. Al Ma-Mari, D.M. Bracher, A. Kleibert, M.C. Rosamond, E.H. Linfield, T.A. Moore, J. Raabe, G. Brunell, C. H. Marrows, Discrete Hall resistivity contribution from Néel skyrmions in multilayer nanodiscs, Nat. Nanotech. 13 (2018) 1161.
[18] D. Macciarello, W. Legrand, N. Reyren, K. Garcia, K. Bouzehouane, S. Collin, V. Cros, A. Fert, Electrical detection of single magnetic skyrmions in metallic multilayers at room temperature, Nat. Nanotech. 13 (2018) 233.
[19] A. Vansteenkiste, J. Leliaert, M. Dvornik, M. Helsen, F. Garcia-Sanchez, B. V. Waeyenberge, The design and verification of MuMax[3], AIP Adv. 4 (2014), 107133.
[20] J.S. Moodera, L.R. Kinder, Ferromagnetic-insulator-ferromagnetic tunneling: Spin-dependent tunneling and large magnetoresistance in trilayer junctions, J. Appl. Phys. 79 (1996) 4224.
[21] K. Zeissler, S. Finizio, C. Barton, A.J. Huxtable, J. Massey, J. Raabe, A. D. Sadovnikov, R. Brearton, T. Hesjedal, G. van der Laan, M.C. Rosamond, E. H. Linfield, G. Burnell, C.H. Marrows, Diameter-independent skyrmion Hall angle observed in chiral magnetic multilayers, Nat. Commun. 11 (2020) 428.
[22] X.S. Wang, H.Y. Yuan, X.R. Wang, A theory on skyrmion size, Commun. Phys. 1 (2018) 31.
[23] R. Juge, S.G. Je, D.D.S. Chaves, I.D. Buda-Prejbeanu, J. Pena-Garcia, J. Nath, I. M. Miron, K.G. Rana, L. Aballe, M. Foerster, F. Genuzio, T.O. Mentes, A. Locatelli, F. Maccherozzi, S.S. Dhesi, M. Belmeguenai, Y. Roussigné, S. Auffret, S. Pizzini, G. Gaudin, J. Vogel, O. Boulle, Current-driven skyrmion dynamics and drive-dependent skyrmion hall effect in an ultrathin film, Phys. Rev. Appl 12 (2019), 044007.
[24] B. Parks, A. Abdelgawad, T. Wong, R.F.L. Evans, S.A. Majetich, Magnetoresistance dynamics in superparamagnetic core-shell nanodots, Phys. Rev. Appl. 13 (2020), 014063.